Journal of the European Ceramic Society 22 (2002) 101–107

www.elsevier.com/locate/jeurceramsoc

Evaluation of degradation of thermal barrier coatings using impedance spectroscopy

Md Shawkat Ali, Shenhua Song, Ping Xiao *

Materials Group, Department of Mechanical Engineering, Brunel University, Uxbridge, Middlesex UB8 3PH, UK

Received 9 December 2000; received in revised form 8 February 2001; accepted 16 February 2001

Abstract

In this work, impedance spectroscopy (IS) has been used to evaluate the degradation of thermal barrier coatings (TBCs) due to oxidation at 1150°C. The spallation of TBCs was found to be induced by the development of thermally grown oxides (TGO) produced from the oxidation of TBCs. The change in the electrical properties of the TGOs was found to be related to the change in the microstructure and microchemistry of the TGO. The resistivity of the TGO due to oxidation from 10 to 1000 h decreased rapidly, which corresponded to the increase in porosity in the TGO and the compositional change of the TGO from α-Al_2O_3 to a mixture of α-Cr_2O_3 and $(Ni,Co)(Cr,Al)_2O_4$ spinel. The slow decrease in the resistivity of the TGO from oxidation for 1000–2000 h indicated that there was little change in the composition of the mixed oxides, although the growth rate of the TGOs was relatively fast during this oxidation period. The disappearance of α-Al_2O_3 in the TGO caused a rapid oxide growth during oxidation and led to the spallation of TBCs.

Keywords: Al_2O_3; Coatings; Cr_2O_3; Impedance spectroscopy; $(Ni,Co)(Cr,Al)_2O_4$; Oxidation; Thermal barrier coatings

1. Introduction

Thermal barrier coatings (TBCs) on turbine blades have been used for increasing turbine engine operation temperatures.[1–5] A TBC system typically consists of a metallic bond coat on a superalloy substrate and a ceramic top coat. An yttria stabilised zirconia (YSZ) (6–8 wt.% Y_2O_3, balance% ZrO_2) is normally used as a top coat for thermal insulation. A bond coat consisting of a MCrAlY (M = Ni and/or Co) alloy is used to increase the adhesion of YSZ and to protect the superalloy substrate from oxidation by forming a continuous protective oxide scale (usually α-Al_2O_3) between the bond coat and YSZ. As the thermally grown oxide (TGO) grows at the YSZ/bond coat interface due to the oxidation of bond coat, internal stresses are built up at the top coat/bond coat interface as the oxidation is accompanied with volumetric expansion. The thermal mismatch among the bond coat, TGO and YSZ further increases the stress level during thermal cycling of TBCs. These stresses can cause cracking in the YSZ and lead to failure of TBCs.[2,6–8] It has been found that the growth of TGO layer is an important factor in controlling the degradation of TBCs.[2,9] However, it is difficult to examine the degradation of TBCs non-destructively, which is essential for predicting the lifetime and failure of TBCs on engine components.

Acoustic emission has been used for the examination of cracking in TBCs,[10] where acoustic emissions are pulses of the elastic strain energy released spontaneously during deformation. Infrared thermography has been used[11,12] for evaluating the delamination of TBCs. In this case, a pulse of heat is applied to one side of a specimen, then the spatial distribution of the heat flux on the opposite surface, which is dependent on the homogeneity of the specimen, is measured. Piezospectroscopy has been developed to examine the stress level and failure in TBCs non-destructively, based on the analysis of the shape of the luminiescence spectra.[13] Although these non-destructive techniques can be used to characterise the formation of defects in TBCs when cracking occurs, these techniques cannot be used to determine the extent of degradation and predict the failure of TBCs. None of these techniques can be used to determine the composition

* Corresponding author. Fax: +44-1895-256392.
E-mail address: ping.xiao@brunel.ac.uk (P. Xiao).

0955-2219/01/$ - see front matter
PII: S0955-2219(01)00234-5

and growth of the TGO, even though the growth of the TGO is a critical factor in controlling the degradation of TBCs.[14,15] Impedance spectroscopy is a non-destructive technique, which has been used extensively to determine electrical properties of materials.[14–17] Since YSZ is an ionic conductor, whereas the TGO is normally an insulator, impedance spectroscopy can be used to examine the composition change and microstructural development of the TGO in TBCs by measuring impedance spectra of TBCs. It is anticipated that changes in the electrical properties of TGO are closely associated with its microstructure and microchemistry. As a consequence, the TGO growth in TBCs can be evaluated by using impedance measurements of TBCs.

The aim of the present work is to develop impedance spectroscopy as a non-destructive tool for evaluating the degradation of TBCs. It has been found that the results from impedance measurements could be related to the growth phenomena of the TGO. Therefore, the degradation of TBCs controlled by the growth of the TGO, can be monitored non-destructively using impedance spectroscopy.

2. Experimental procedure

TBC samples of size $10\times10\times20$ mm were prepared by Sermatech Ltd, Lincoln, UK. Both bond coat ($\sim$150 μm thick) and top coat ($\sim$250 μm thick) were applied using plasma spray to Haynes-230 superalloy plates. Chemical composition of the Haynes-230 superalloy in wt.% is 22Cr, 14W, 3Fe, 2Mo, 0.02La, 0.015B and 0.1C, balanced by nickel. Chemical composition of the bond coat in wt.% is 21Cr, 8Al, 38.5Co, 32Ni, and 0.5Y. The YSZ contains 8 wt.%Y_2O_3 and 92 wt.%ZrO_2. During thermal cycling, the samples were kept at 1150C in air for 10, 100, 200, 1000, 1500 and 2000 h, respectively. Both the heating and cooling rates were 10°C min^{-1}. Six thermal cycles were carried out for the 2000 h-oxidised samples with dwell periods of 100 h (cycles 1 and 2), 300 h (cycle 3) and 500 h (cycles 4, 5 and 6), respectively. Five thermal cycles were carried out for the 1500 h-oxidised samples with dwell periods of 100 h (cycles 1 and 2), 300 h (cycle 3), and 500 h (cycles 4 and 5), respectively. Four thermal cycles were carried out for the 1000 h-oxidised samples with dwell periods of 100 h (cycles 1 and 2), 300 (cycle 3) and 500 h (cycle 4), respectively. Two thermal cycles were carried out for the 200 h-oxidised samples with dwell periods of 100 h. One thermal cycle was carried out for the 100 and 10 h-oxidised samples.

For impedance measurements, the oxide layer formed at the surface of the Hanes-230 alloy substrate without TBCs was mechanically polished off to expose the metal substrate acting as an electrode. The TBC surface was cleaned in an ultrasonic bath with acetone and painted with a silver conductive paint acting as another electrode. The electrode area (painted area) was 5×5 mm square. The silver paint was fired in air at 450°C for 30 min to increase the adhesion of the paint to the TBC. Impedance measurements were conducted using a Solartron SI 1255 HF frequency response analyser coupled with a Solartron 1296 Dielectric Interface, which is computer-controlled. Spectra analysis was performed by using a Zview impedance analysis software (Scribner Associates Inc, Southern Pines, NC) to extract the electrical and dielectric properties of TBCs. In the measurements, an AC (alternating current) amplitude of 10 mV was employed and the AC frequency was in the range of $1–1\times10^7$ Hz. The measurements were performed at 400°C on three samples for each oxidation condition. The average values of electrical properties obtained from the measurements were taken as the experimental results.

A J840 scanning electron microscope (SEM) coupled with an energy dispersive X-ray (EDX) microanalyzer was employed to characterise the TGO. Crystal structures of the TGO were determined using X-ray diffraction technique.

3. Results and discussion

3.1. Impedance measurements

In impedance measurements, a sinusoidal potential perturbation is applied to the test electrodes, which are in contact with the relevant TBC. Impedance diagrams are acquired by measuring the magnitude and phase shift of the resulting current. There are two types of impedance diagrams, namely Nyquist plots and Bode plots. In a Nyquist plot, the impedance is represented by a real part Z' and an imaginary part Z'' with the formula $Z(w) = Z' + jZ'$, where $j = \sqrt{-1}$. Therefore, the Nyquist plot is also termed the complex plane impedance plot. In a Bode plot, the modulus of the impedance and the phase angle are both plotted as a function of frequency. For a simple resistor-capacitor (R–C) circuit, the Nyquist plot is characterised by a semicircle. Usually, the Nyquist plot is used to determine the major parameters, such as resistance and capacitance corresponding to an electrochemical system. In a Nyquist plot that contains only one semicircle, the resistance value, R, is determined directly from the intercept with the real Z axis. If the system is complicated, there may be a few semicircles present. In this scenario, the spectra have to be fitted with an equivalent circuit model, which is representative of the microstructural features of the materials under examination.[15,18]

Typical Nyquist plots for the samples oxidised for different times are represented in Fig. 1. Two semicircles are present in each Nyquist plot, corresponding to two

layers in the TBC. One of the two layers is the YSZ top coat and the other is the TGO layer. It has been confirmed[19,20] that the high-frequency semicircle (on the left hand side) corresponds to the YSZ top coat and the low-frequency semicircle (on the right hand side) corresponds to the TGO layer.

To obtain the electrical properties of the TGO layer, it is necessary to establish an equivalent circuit model for fitting the measured impedance spectra. The two semicircles can be simulated based on a model of two R–C components with a series connection (Fig. 2). In the model, CPE is the constant phase element which is more suitable to describe the behaviour of a non-ideal capacitor where capacitance depends on frequency.[15] This is because the surface of electrodes is rough, which may cause a frequency dispersion due to heterogeneous current density distribution, i.e. C is not an ideal capacitor. The effect of inhomogeneous materials on capacitance has been discussed in previous studies.[21,22] The current research was only concerned with the conductivity of TBCs rather than the dielectric properties, therefore, the details on the CPE have not been provided. A simulation result is shown in Fig. 3, together with a measured spectrum. Both simulation and measured results fit very well. The resistance obtained from the simulation was therefore taken as the measured result. The resistivity of the TGO was calculated after the TGO thickness was determined using SEM.

The resistance and resistivity of the TGO are as a function of thickness with the oxidation time given for each data point (Fig. 4). Clearly, the resistance of the TGO increased with increasing thickness of the TGO from 1 to 10 h oxidation. However, the resistance then decreased as the oxidation time approached 1000 h. The resistance appeared to stabilise after 1000 h. The resistivity showed little change in the TGO during oxidation between 1 and 10 h, which indicated that the composi-

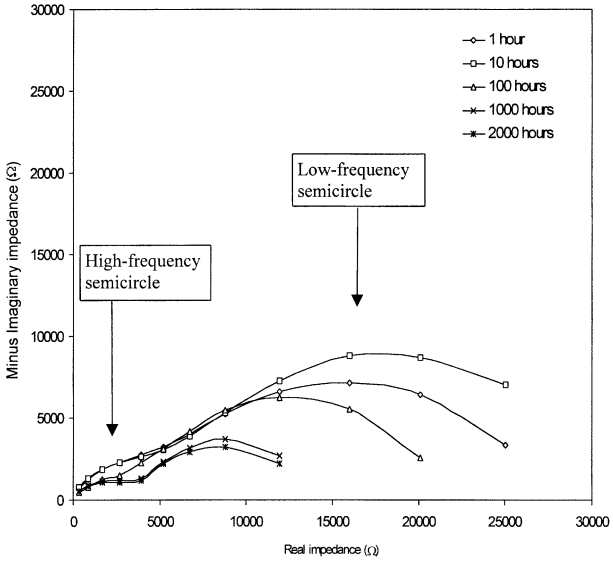

Fig. 1. Nyquist plots for the samples oxidised in air at 1150°C for different periods.

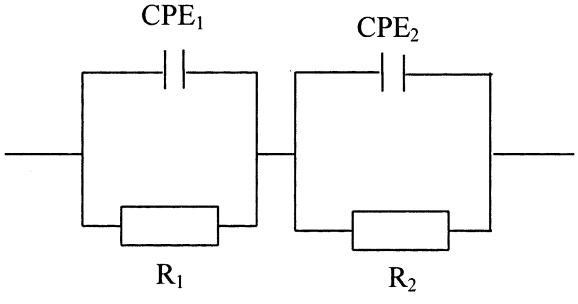

Fig. 2. Equivalent circuit model for a TBC system.

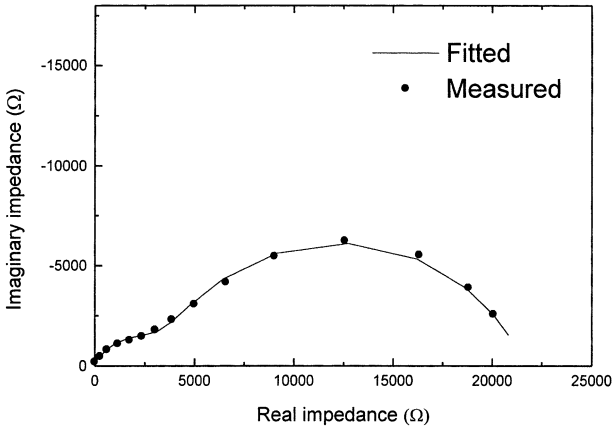

Fig. 3. Simulation spectra based on the equivalent circuit model and the measured spectra of the sample oxidised in air at 1150°C for 100 h.

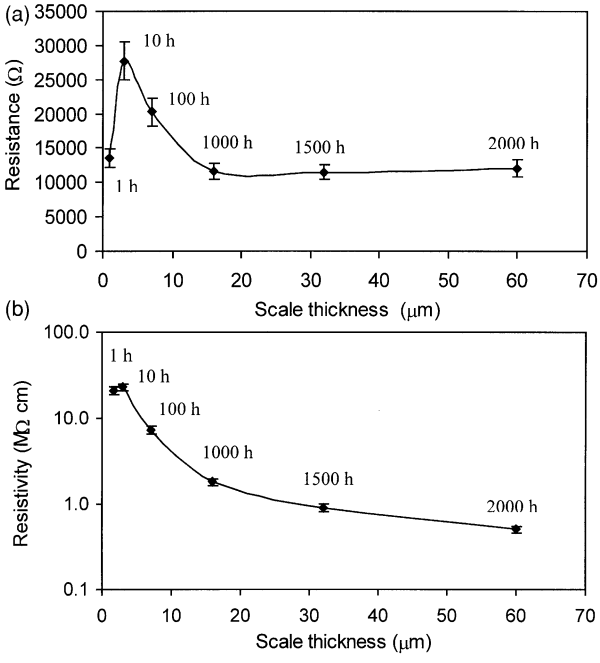

Fig. 4. (a) Resistance versus the thickness of the TGO and (b) resistivity versus the thickness of the TGO, with the oxidation time indicated on each data point.

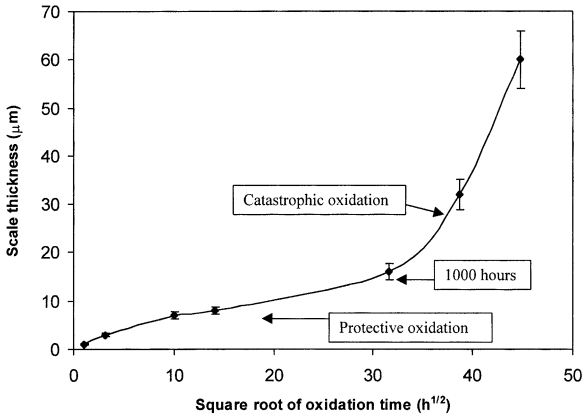

Fig. 5. Thickness of the TGO vs. oxidation time for the TBC coated sample.

tion and microstructure of the TGO altered little during this oxidation period. However, the resistivity of the TGO decreased with increasing oxidation time. It should be noted that the rate of reducing resistivity is much higher between 10 and 1000 hours than that between 1000 and 2000 h. This implies that the composition of the TGO changes considerably during this oxidation period, which can lead to a fast growth of TGO.

3.2. TGO growth

The oxidation kinetics of the bond coat, shown in Fig. 5, follows the parabolic law until 1000 h. During oxidation times less than 1000 hrs, the TGO acts as a protective layer, thus the TGO growth rate is relatively

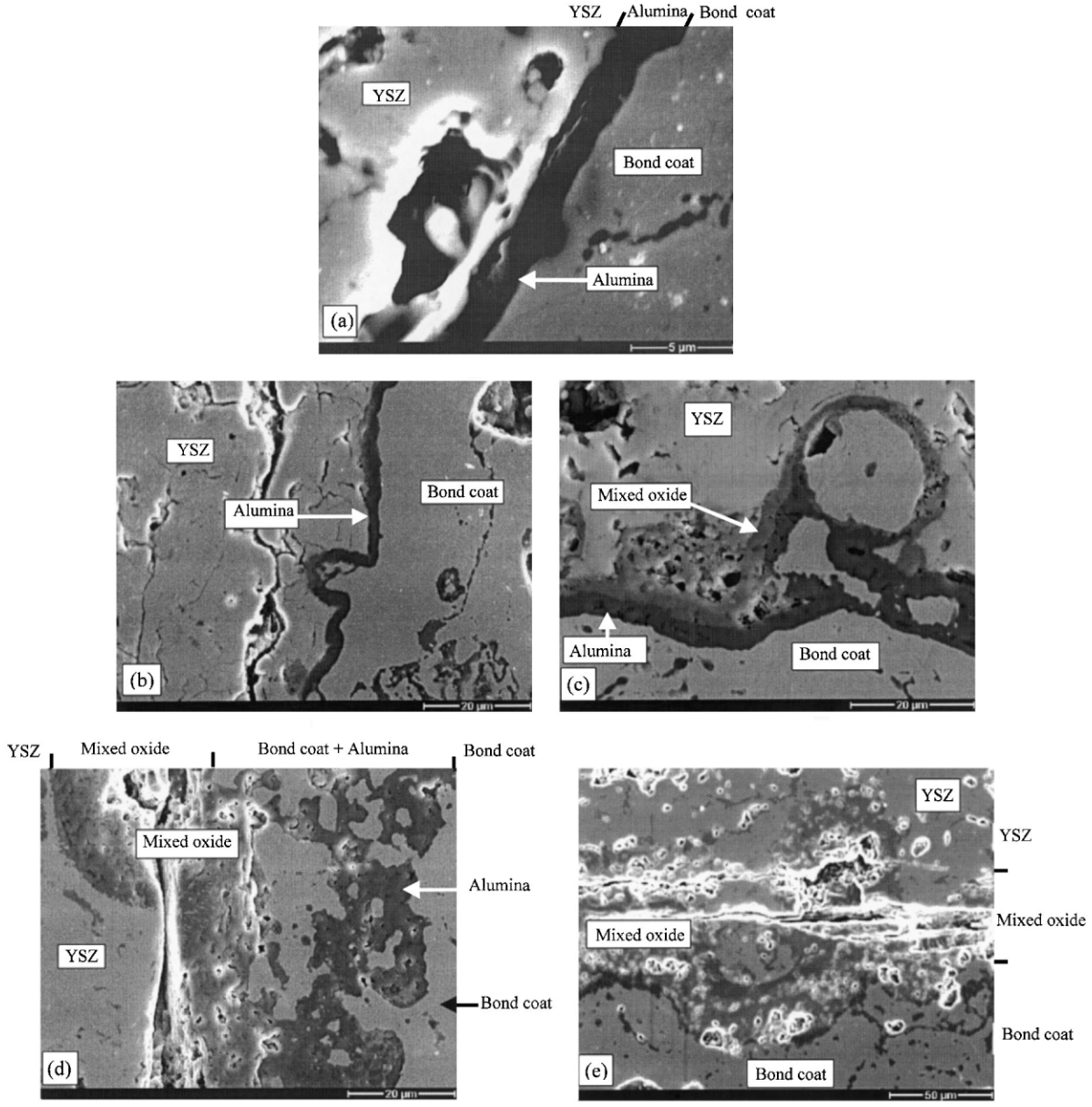

Fig. 6. SEM images of the cross-sections of the samples oxidised in air at 1150°C for (a) 1 h, (b) 10 h, (c) 100 h, (d) 1000 h and (d) 2000 h.

low. Further oxidation leads to a substantial increase in the growth rate of the TGO. As a result, the failure of TBCs occurred due to the considerable increase in the thickness of the TGO. Fig. 6 shows the cross-sections of TBCs after oxidation for different periods. In both 1 and 10 h-oxidised samples, the TGO is mainly a dense dark-coloured oxide layer, although a small amount of grey-coloured oxide appears between the dark oxide layer and YSZ in the 10 h-oxidised sample (Fig. 6b). In the 100 hr-oxidised sample, the dark-coloured oxide layer is accompanied with a layer of porous grey-coloured oxide near the YSZ (Fig. 6c). It appears that the dark oxide layer in the 100 h-oxidised sample is more porous than that in the 10 h-oxidised sample. After 1000 h oxidation, the dark oxide has almost disappeared and replaced by a porous grey oxide layer (Figs. 6d and 6e). The formation of the porous TGO promotes the rapid growth of the TGO after 1000 h oxidation. In addition, some dark oxides were formed inside the bond coat as a result of internal oxidation.

XRD analysis of the TGO was conducted after the spallation of the YSZ top coat (Fig. 7). The analysis indicated the presence of $(Ni,Co)(Cr,Al)_2O_4$ spinel, α-Al_2O_3, α-Cr_2O_3, and YSZ. Fig. 8 shows the elemental composition in the oxide layers which was determined using EDX microanalysis. The microanalysis in conjunction with the XRD analysis suggested that the dark layer mainly contained α-Al_2O_3 in the samples oxidised for less than 1000 h, while for more than 1000 h oxidation, α-Al_2O_3 and α-Cr_2O_3 were the major phases present in this layer. The grey layer in the TGO mainly consisted of Al, Cr, Ni and Co. In the samples oxidised for less than 1000 h, the contents of Al, and Co in the grey layer increased while the content of Cr and Ni decreased slightly (Fig. 8). After oxidation for 1000 h, the content of Al_2O_3 in both the dark and grey layers decreased while the content of Cr_2O_3 increased with increasing oxidation time (Fig. 8), leading to the disappearance of the dark Al_2O_3 layer. Both EDX and XRD results suggest that the grey layer is mainly composed of $(Ni,Co)(Cr,Al)_2O_4$ spinel, α-Al_2O_3 and α-Cr_2O_3 when the oxidation time is shorter than 1000 h and of $(Ni,Co)(Cr,Al)_2O_4$ spinel and α-Cr_2O_3 when the oxidation time is longer than 1000 h. The YSZ detected by XRD should be the top coat retained on the TGO after the spallation of YSZ, which was also reported by Shillington and Clarke.[23] The composition and microstructural change in the TGO may be caused by the depletion of Al in the bond coat, which would be due to the formation and growth of Al_2O_3 at the bond coat/YSZ interface. Therefore, the less active elements, Cr, Ni and Co, formed α-Cr_2O_3 and $(Ni,Co)(Cr,Al)_2O_4$ spinel, which further increased the stress in TBCs and induced cracking in the TGO. The high porosity and presence of microcracks in the mixed oxide layer promoted the formation of α-Cr_2O_3 and spinel by providing a fast route for oxygen transport and surface diffusion of metal and oxygen ions. It appears that the Cr, Ni, and Co diffused through the Al_2O_3 layer to form α-Cr_2O_3 and $(Ni,Co)(Cr,Al)_2O_4$ spinel. Oxygen also penetrated through Al_2O_3 layer to reach the bond coat and produced oxides inside the bond coat. In addition, the Al_2O_3 layer seemed to dissolve into the mixed oxides gradually and finally disappeared. It is unclear why a mixed oxide layer is not formed at the bond coat/alumina interface.

Fig. 6 shows that cracks initiated and propagated in the mixed grey oxide layer adjacent to the YSZ layer in

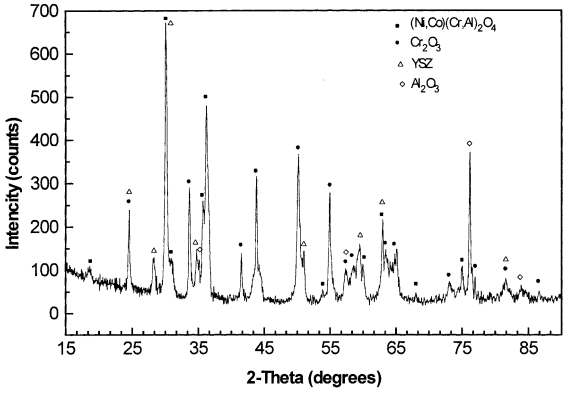

Fig. 7. X-ray diffraction pattern from the TGO on the bond coat in the samples oxidised in air at 1150°C for 2000 h.

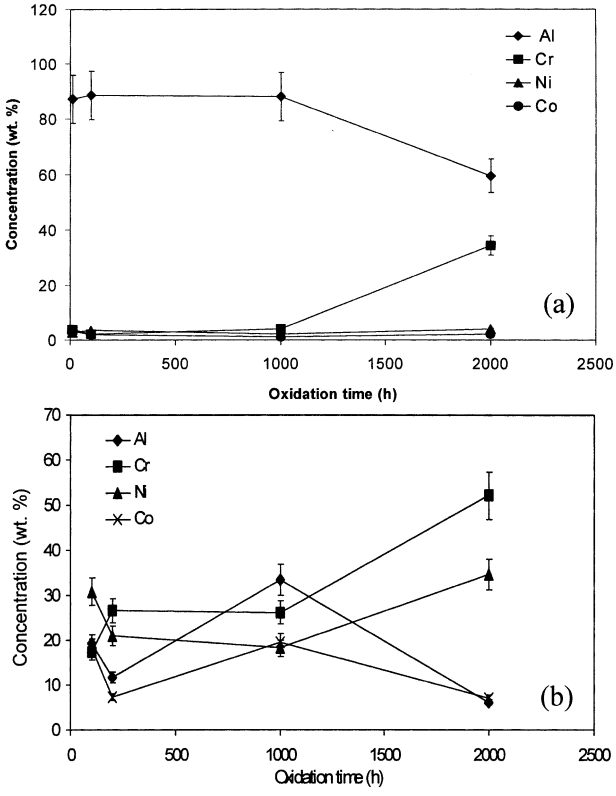

Fig. 8. EDX microanalysis for (a) the dark oxide layer and (b) the grey oxide layer in samples oxidised in air at 1150°C for different periods.

parallel with the coat/substrate interface. The internal stress generated by the oxide growth as well as the thermal expansion mismatch between different oxide layers should be responsible for the formation of cracks.[24] Samples that were oxidised for a longer period exhibited more severe porosity in the grey mixed oxide layer (Fig. 6), which weakens the strength of the oxide layer and produced more cracks. This porosity may be caused by the evaporation of CrO_3 gas during high temperature oxidation.[25,26] As is well known,[25,27], α-Cr_2O_3 and $(Ni,Co)(Cr,Al)_2O_4$ spinel are p-type semiconductors. Their conductivity is determined by electron hole conduction. The electron hole concentration, as described in Ref. 28 increases with increasing oxygen partial pressure. Normally, the oxygen partial pressure decreases from the outer surface of the oxide scale to the scale-substrate interface. The increase in porosity and cracks may lead to an increase in oxygen partial pressure within the scale, giving rise to an increase in electron hole concentration and in turn an increase in conductivity. Our previous work on NiO has also confirmed this phenomenon.[29]

3.3. Relation between impedance spectra and the TGO growth

According to the microstructural analysis of the TBCs, the Nyquist plot from impedance measurements of the TBCs should show three semicircles corresponding to YSZ, mixed oxide layer and alumina layer, respectively. However, only two semicircle spectra appeared in the measured impedance diagram (Fig. 1). The high frequency semicircle (left) corresponds to YSZ, as discovered in previous studies.[19,20] Therefore, the low frequency semicircle should correspond to the mixed oxide and alumina layers. The disappearance of one semicircle may be caused by the lack of two distinguished and continuous layers in the mixed oxide and alumina. During oxidation at the early stage, although the alumina layer was continuous, the mixed oxides were patchy. As oxidation continued, the alumina changed its composition and gradually dissolved into the mixed layer, but the mixed oxide then became a continuous layer. As a consequence, the TGO are represented by one electrical unit, which corresponds to one semicircle in the impedance spectra.

It should be noted that the resistivity of the TGO decreased rapidly after 10 h-oxidation (Fig. 4) whereas the oxidation growth rate increased rapidly after oxidation for 1000 h (Fig. 5). To explain this phenomena, the relation between the resistivity of oxide and the oxide growth rate should be established. The growth behaviour of the TGO until oxidation for 1000 h follows the parabolic law. The parabolic growth rate constant can be expressed as[28]

$$k_r \sim \sigma_e\sigma_i/(\sigma_e + \sigma_i)$$

where σ_e and σ_i are the electronic and ionic conductivities.

If $\sigma_e >> \sigma_i$, k_r will be mainly determined by σ_i. On the other hand, the electrical conductivity σ is mainly determined by σ_e, since $\sigma = \sigma_i + \sigma_e$. In this case, the growth rate of the oxide should be determined by the diffusion of ions and independent of the electrical conductivity. As mentioned above, both α-Cr_2O_3 and $(Ni,Co)(Cr,Al)_2O_4$ spinel are electronic hole semiconductors and their electronic conductivity is much higher than its ionic conductivity. α-Al_2O_3 is normally regarded as an insulator and it is unclear whether its electronic conductivity is dominant. Here we attempt to estimate the ionic conductivity of Al_2O_3, in comparison with its electrical conductivity. The ionic conductivity, σ_i, can be evaluated by[30]

$$\sigma_i = \frac{C_i Z_i^2 e^2 D_i}{kT} \quad (1)$$

where C_i is the vacancy concentration (the number of vacancies per unit volume). Z_i is the valance number (3 for Al and 2 for O), e is the charge (1.60×10^{-19} C), D_i is the diffusion coefficient for ions, k is the Boltzmann constant, and T is the absolute temperature. The atomic fraction of vacancies in thermal equilibrium, n_i, can be calculated by[30]

$$n_i = \exp\left(\frac{-E_v}{2kT}\right) \quad (2)$$

where E_v is the vacancy formation energy. The E_v for Al and O ions in α-Al_2O_3 is 6.2 and 6.1 eV, espectively.[30] The atomic fractions of vacancies for Al and O ions are obtained as 1.3×10^{-11} and 2.0×10^{-11} respectively at 1150°C and 1.0×11^{-23} and 3.6×10^{-25} at 400°C. It should be noted that the oxidation temperature and the temperature for impedance measurements are 1150 and 400°C, respectively. The diffusion coefficients for Al and O ions are 2.2×10^{-18} and 5.0×10^{-26} m^2 s^{-1} at 1150°C and 1.0×10^{-25} and 5.6×10^{-33} m^2 s^{-1} at 400°C.[30] Based on the above data, the ionic conductivities for Al^{3+} and O^{2+} in Al_2O_3 were calculated as 1.6×10^{-17} and 9.1×10^{-21} Ω^{-1} m^{-1} at 1150°C and 1.2×10^{-34} and 1.7×10^{-44} Ω^{-1} m^{-1} at 400°C. The electrical conductivity (combining electronic and ionic conductivity) of α-Al_2O_3 was reported as about 10^{-5} Ω^{-1} m^{-1} at 1150°C and 10^{-10} Ω^{-1} m^{-1} at 400°C.[31] Clearly, the electronic conductivity is dominant in the electrical conduction of α-Al_2O_3 and, therefore, its growth rate is controlled by the diffusion of Al ions in the oxide. The reason for the TGO to grow rapidly after 1000 h oxidation is that the metal diffusion rate in the TGO became faster after disappearance of alumina in the TGO.[30] It should be noted that all of the calculations made above were based on thermal equilibrium condition

both at 400 and 1500°C. We should also indicate that there was no change shown in the impedance spectra of TBCs during the impedance measurements at 400°C, which suggests that the defect concentration in the oxides reached the local equilibrium condition.

As described above, the resistivity for the electron hole semiconductors like the oxides found in this work decreases with increasing porosity/cracks. As a consequence, the fast decrease in resistivity during oxidation from 10 to 1000 h may also be due to the increase in porosity/cracks in the TGO during oxidation. The slow decrease in resistivity after 1000 h oxidation may be due to a small change in microstructure and composition in the TGO, even though the thickness of the TGO increased rapidly. Therefore, the resistance measurement is more sensitive to the change in composition and porosity/cracks in the TGO, rather than the thickness of the TGO. It should be noted that the oxidation temperature adopted in this work (1150°C) is much higher than the actual bond coat operating temperature (900–1000°C). The oxidation of TBCs at lower temperatures would produce a TGO of different composition and microstructure. Therefore, different impedance measurement results should be obtained.[19,20] By combining our understanding of oxidation behaviour of bond coat and determining impedance spectra of TBCs, it is very promising to determine the degradation status of TBCs non-destructively using impedance spectroscopy.

4. Summary

Impedance spectroscopy has been used to evaluate the degradation of TBCs at 1150°C. The microstructual and composition changes in the TGO at the metal/YSZ interface induced the degradation and failure of TBCs. The TGOs changed gradually from Al_2O_3 to a mixture of α-Cr_2O_3 and $(Ni,Co)(Cr,Al)_2O_4$ spinel, which corresponds to the changes in electrical properties. The resistivity of the TGO decreased gradually with increasing prorosity and the compositional change of the TGO from Al_2O_3 to a mixture of α-Cr_2O_3 and $(Ni,Co)(Cr,Al)_2O_4$ spinel, even though the thickness of TGO increased considerably. Therefore, the impedance measurements are more sensitive to compositional and microstructural changes in the TGO, rather than thickness of the TGO.

Acknowledgements

The authors gratefully acknowledge the assistance of Dr. Adrian Sanders (Alstom Gas Turbine Ltd) for supplying samples and would also like to express gratitude to EPSRC and Alstom Gas Turbine Ltd for jointly funding the work at Brunel University.

References

1. Kool, G. A., *ASME Tech. Paper 94-gt-475*. Mechanical Engineers, New York, 1994.
2. Haynes, J. A., Rigney, E. D., Ferber, M. K. and Porter, W. D., *Surf. Coat. Technol.*, 1996, **86–87**, 102.
3. Miller, R. A., *J. Thermal Spray Technol.*, 1997, **6**, 35.
4. Bose, S. and DeMasi-Marcin, J., *J. Thermal Spray Technol.*, 1997, **6**, 99.
5. Sergo, V. and Clarke, D. R., *J. Am. Ceram. Soc.*, 1998, **81**, 3237.
6. Jones, R. L., *Mater. High. Temp.*, 1991, **9**, 228.
7. Hendricks, R. C., McDonald, G. and Mullen, R. L., *Ceram. Eng. Sci. Proc.*, 1983, **4**, 802.
8. Jones, R. L. and Mess, D., *Surf. Coat. Technol.*, 1996, **86–87**, 94.
9. He, M. Y., Evans, A. G. and Hutchinson, J. W., *Mater. Sci. Eng. A*, 1998, **A245**, 16.
10. Berndt, C. C., *J. Eng. Gas Turbine and Power*, 1985, **107**, 142.
11. Harada, S., Ikeda, Y., Mizuta, Y. and Sugita, Y and Ito, A., The inspection of delaminated defects in ZrO_2 coated material by infrared thermography techniques. In *Proceedings of the Int. Symposium on Thermographic NDT and E Techniques Symposium*, 1995, pp. 47–52.
12. Saitoh, M., Itoh, Y. and Ishii, J., Evaluation of thermal barrier coating using infrared thermography. In *Proceedings of the Int Symposium on Thermographic NDT and E Techniques Symposium*, 1995, pp. 53–58.
13. Xiao, P. and Clarke, D. R., *J. Am. Ceram. Soc.*, 2000, **83**, 1165.
14. Mansfeld, F., *Corrosion*, 1981, **36**, 301.
15. MacDonald, J. R., *Impedance Spectroscopy*. John Wiley & Sons, Chichester, 1987.
16. Cogger, N.D. and Evans, N.J., An Introduction to Electrochemical Impedance Measurement. Technical Report Number 006, Solartron Ltd, Farnborough, UK, 1998.
17. Allen, J. B. and Faulkner, L. R., *Techniques Based on Concepts of Impedance, Electrochemical Methods (Fundamentals and Application)*. John Wiley & Sons, Chichester, 1980 (Chapter 9).
18. Fletcher, J. G., West, A. R. and Irvine, J. T. S., *J. Electronchem. Soc.*, 1995, **142**, 2650.
19. Wang, X., Mei, J. F. and Xiao, P., *J. Mater. Sci. Lett.*, 2001, **20**, 47.
20. Wang, X., Mei, J. F. and Xiao, P. Non-destructive evaluation of thermal barrier coatings using impedance spectroscopy. *J. Mater. Sci.*, submitted.
21. Delouis, C., Lafont, M. C., Pebere, N. and You, D., *Corrosion Sci.*, 1993, **34**, 1567.
22. Rammelt, U. and Reinhard, G., *Electrochim. Acta*, 1994, **40**, 505.
23. Shillington, E. A. G. and Clarke, D. R., *Acta Mater.*, 1999, **47**, 1297.
24. Schutze, M., *Protective Oxide Scales and Their Breakdown*. John Wiley & Sons, Chichester, 1997.
25. Kubaschewski, O. and Hopkins, B. E., *Oxidation of Metals and Alloys*, 2nd edn. Butterworths, London, 1967.
26. Graham, H. C. and Davis, H. H., *J. Am. Ceram. Soc.*, 1971, **54**, 89.
27. Alper, A. M., *High Temperature Oxides, Part 1: Magnesia, Lime, and Chrome Refractories*. Academic Press, New York, 1970.
28. N. Birks and Meier, G.H. *Introduction to High Temperature Oxidation of Metals*, Edward Arnold, London, 1983.
29. Song, S.-H. and Xiao, P., Microstructural evolution of the oxide film formed during high temperature oxidation of nickel evaluated by means of impedance spectroscopy. *Scripta Mater.*, in press.
30. Chiang, Y.-M., Birnie, D. P. and Kingery, W. D., *Physical Ceramics*. John Wiley and Sons, New York, 1997.
31. Samsonov, G. V., *The Oxide Handbook*. IFI/Plenum, London, 1973.